Impregnation and delignification during kraft pulping of hardwood chips: characterization using in-situ X-ray tomography

Wood Science and Technology (2026) 60:52
https://doi.org/10.1007/s00226-026-01767-6

ORIGINAL

Impregnation and delignification during kraft pulping of hardwood chips: characterization using *in-situ* X-ray tomography

Carolina Marion de Godoy[1] · Endri Laçaj[2] · Klara Hackenstrass[3] · Luigi Galluccio[1,4] · Haiyang Yu[3] · Sara Florisson[3] · Malin Wohlert[3] · Stephen A. Hall[2] · Merima Hasani[1,4] · Hans Theliander[1,4]

Received: 7 January 2026 / Accepted: 11 March 2026

Abstract

In this paper, *in-situ* X-ray microtomography was used to analyze liquor penetration/impregnation and delignification of wood chips during kraft pulping, allowing microstructural changes to be assessed over time. The study was conducted with sapwood of three hardwood species (alder, aspen and birch), using a reactor designed to provide liquor circulation and temperature control. Each wood sample was digested at 141 °C for four hours and, throughout this time, fifteen 3D images of the central portion of the samples were acquired. The images were segmented and used to measure lumen size, cell wall thickness and wood chip porosity. The results confirmed that vessels offered the preferred path for liquor penetration in the hardwoods. Moreover, liquor penetration from ray cells to adjacent fibers was shown to be a less efficient path for impregnation. Regarding delignification, fiber separation began first in aspen and last in alder, and the complete separation took between 1 and 1.5 h to occur in the center of the samples. The porosity of the chips increased continuously after liquor penetration, whereas cell wall thickness decreased more substantially during fiber separation, especially in aspen, but remained relatively stable afterwards. Furthermore, the position of the fibers in relation to vessels and rays did not impact the rate of delignification significantly. Overall, this work shows that *in-situ* tomography can be a valuable technique to move forward research on wood impregnation and on topochemistry of lignin removal during pulping.

Extended author information available on the last page of the article

Published online: 16 April 2026

Introduction

Ensuring uniform delignification of wood is vital during the production of kraft pulp. A heterogeneous distribution of lignin in the pulp affects properties such as tensile strength and fiber-fiber bonding strength, which can compromise further processing (e.g., papermaking). In addition, nonuniform delignification can result in pulps with high content of shives, and it can lead to high consumption of bleaching agents (Gullichsen et al. 1992; Bacarin et al. 2017). Not surprisingly, understanding how lignin removal progresses inside wood chips has been a topic of extensive research throughout the years (Whiting and Goring 1981; Gustafson et al. 1989; Malkov et al. 2003; Aguayo et al. 2014). In this area of research, two prominent fields include the topochemistry of delignification (i.e., the study of delignification in different fractions of the wood tissue) and the study of wood impregnation.

Proper impregnation of chips with cooking liquor is a key step for achieving the most uniform removal of lignin possible during pulping (Gustafson et al. 1989; Malkov et al. 2003; Brännvall 2018). The impregnation process involves two main mechanisms: liquor penetration and diffusion of cooking chemicals into the wood structure. In hardwoods, the most accepted path for liquor penetration begins in the vessels and spreads through the pits to the lumen of adjacent cells. In addition, ray cells can contribute to short distance lateral penetration, spreading the liquor in the radial direction (Stone and Green 1959; Wardrop and Davies 1961). The diffusion of cooking chemicals occurs due to concentration gradients inside the wood chips. The magnitude of these gradients depends on several variables, including the consumption of chemicals due to neutralization and other reactions, chip thickness, wood morphology, and processing conditions such as temperature and liquor-to-wood ratio (Gustafson et al. 1989; Zanuttini et al. 2005).

The uniformity of lignin removal within a wood chip is also affected by the topochemistry of delignification. In kraft pulping, delignification has been shown to occur faster in the secondary wall than in the middle lamella of fibers (Whiting and Goring 1981). Such behavior, while not fully understood, may be connected to the high degree of swelling of the cell wall under alkaline conditions (Koch et al. 2003; Rehbein et al. 2010; Hubbe et al. 2024). It may also be related to the increased accessibility of lignin in the secondary wall due to the removal of hemicelluloses (Wood et al. 1972; Kerr and Goring 1975; Maloney and Paulapuro 1999). The topochemistry of delignification can also be affected by the heterogeneity of lignin distribution and lignin structure through the wood tissue (Aguayo et al. 2014; Takada et al. 2016, 2021). In hardwoods, the cell walls of vessels and rays are usually thinner than the ones of fibers but have a higher lignin content. Likewise, the lignin concentrations are higher in the middle lamellas when compared to secondary walls (Donaldson 2001). The proportion between guaiacyl and syringyl units also varies between different cells. In general, middle lamellas and the secondary walls of vessels are rich in guaiacyl, whereas secondary walls of fibers are rich in syringyl (Saka and Goring 1988; Donaldson 2001).

Still, despite the numerous attempts to unveil the course of kraft delignification inside wood chips, there are several aspects that could be further explored. For instance, few impregnation and topochemical studies have compared the evolution

of lignin removal in different hardwood species. As a result, the impact of their specific anatomical features on the progression of delignification is not fully understood. Moreover, past topochemical and impregnation research often relied on techniques that demand extensive sample preparation, such as light and UV microscopy, and scanning UV microspectrophotometry (Wardrop and Davies 1961; Wood et al. 1972; Koch et al. 2003; Aguayo et al. 2014). Consequently, these studies suffered from the inability to track the evolution of delignification continuously in one single sample. Therefore, there is still limited understanding of how delignification evolves in different hardwoods.

A promising approach to complement past delignification studies and overcome some of the shortcomings of the aforementioned techniques is the use of *in-situ* X-ray computed tomography (CT) to investigate kraft pulping of different hardwoods. This would enable X-ray imaging of hardwood samples while pulping is underway and under the appropriate processing conditions. X-ray imaging techniques are extremely valuable in the field of wood research, being non-destructive and allowing for multi-dimensional analysis of wood samples with varying degrees of spatial and temporal resolution, depending on the technique (e.g., synchrotron, lab-based, micro or macro scanner). In *ex-situ* experiments, CT was utilized successfully in morphological studies of wood (Koddenberg and Militz 2018; Hu et al. 2022; Fabián-Plesníková et al. 2022; Viljanen et al. 2023), in the evaluation of density variations (De Ridder et al. 2011; Biziks et al. 2019; Martha et al. 2025), and in the assessment of structural changes caused by various processes (Koddenberg et al. 2020; Garskaite et al. 2021; Wagih et al. 2021; Hartwig-Nair et al. 2024), among other investigations. *In-situ* X-ray CT experiments can be considerably more challenging, as they require not only suitable spatial resolution, but also reduced imaging times (i.e., increased time resolution). Additionally, they should be designed to mimic the conditions of the process under study, but without disturbing image acquisition, which means the experimental setup should allow the passage of X-rays and the rotation of the sample (Patterson et al. 2018). Most *in-situ* CT studies with wood have focused on phenomena occurring at mild environmental conditions, like moisture transport and mechanical tests (Forsberg et al. 2008; Mäkinen et al. 2022; Martin et al. 2023; Wang et al. 2025). Hence, the potential of this technique to monitor harsher processes, like pulping, has yet to be fully explored. One encouraging result was achieved by Wagih et al. (2022): they designed a reactor suitable for synchrotron CT and capable of withstanding the conditions utilized in alkaline pulping processes. As a result, changes in the wood structure of spruce could be tracked throughout soda pulping, like the swelling and separation of the cell walls.

In this current work, the same reactor developed by Wagih et al. (2022) was used to investigate kraft pulping. The aim was to utilize *in-situ* X-ray microtomography to monitor the evolution of liquor penetration into and delignification of hardwoods through time, with focus on assessing how different morphological features impact the process. The experiments evaluated the behavior of the least accessible cells within wood chips of three commercially relevant species (*Alnus glutinosa*, *Betula pubescens*, and *Populus tremula*), comparing their structural changes during pulping, including changes in the porosity of the chips and variations in cell wall thickness. These results are particularly relevant to understanding changes in mass transport

resistance during kraft cooking and may be useful, for example, in modeling the delignification of wood chips.

Materials and methods

Sample preparation

Small sapwood chips were prepared from logs of alder (*Alnus glutinosa*), aspen (*Populus tremula*) and birch (*Betula pubescens*). The logs were provided by Södra Skogsägarna and came from trees grown in southern Sweden (ages: alder = 43 ± 2 years old, aspen = 28 ± 1 years old, and birch = 27 ± 1 years old) taken at breast height (approx. 1.2 m).

Two chips of each species were analyzed during the *in-situ* experiments. To prepare them, sapwood parts of the logs were hand sawn into pieces with specific dimensions. The chips were 30 ± 1 mm long, with width of 5 ± 1 mm and thickness of 8 ± 1 mm on top and 5 ± 1 mm on the bottom, as shown in Fig. 1. The specific dimensions were needed to allow mounting the samples onto the reactor and to facilitate the comparison between different hardwoods. After the sawing process, the chips were air dried inside a fume hood (final dry content > 89.0% w/w) and kept at room temperature. Thus, when compared to wood chips produced in industrial chippers, the samples utilized in this study had less cracks in their structure and significantly lower water contents.

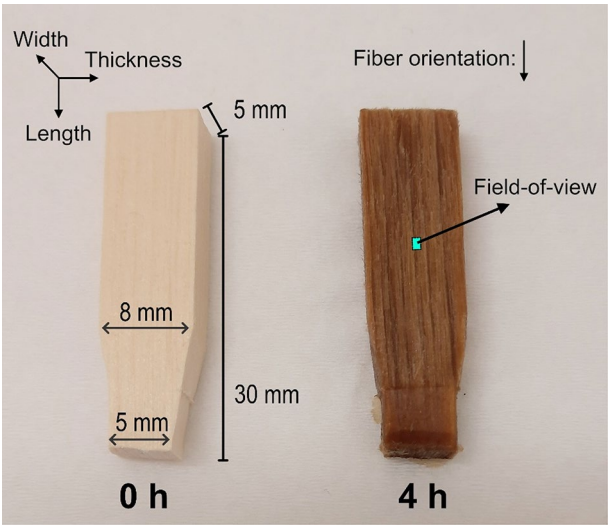

Fig. 1 Hand-cut wood chips of alder before (0 h) and after (4 h) pulping. The main dimensions of the chips and the region observed via tomography are indicated directly in the picture

Kraft cooking

Batch kraft cooking experiments were conducted inside a small reactor (Fig. 2) suitable for *in-situ* testing using synchrotron X-ray CT. The system included a sample holder, a safety valve, a heater coil connected to a temperature controller, a magnetic drive gear pump to circulate the liquor inside the cell, an external cover, and a sample cover. Both covers were made of polyether ether ketone (PEEK) to allow a high transmission of X-rays and no interaction with the pulping chemicals. A more detailed description of the reactor is provided by Wagih et al. (2022).

The cooking experiments were conducted at the ForMAX beamline (MAX IV Laboratory, Lund, Sweden) and X-ray CT was used for *in-situ* monitoring of the kraft process. The reactor was initially assembled in a supporting lab. One wood chip was placed on the sample holder and white liquor was added to the system until the sample cover was completely submerged. Next, the pump was activated (circulation = 24 mL/min) and the temperature controller was set to 60 °C. The system was left open (Fig. 2a) under these conditions for 10 min to allow most of the air to leave the cell. After 10 min, the pump and the heating system were turned off. The cell was closed by securing the safety valve on top of the external cover, and the system was taken to the beamline.

After mounting the reactor on the beamline stage (Fig. 2b), the cooking experiment began by activating the pump and setting the temperature controller to 141 °C (the system took approximately 10 min to reach the set point). It must be noted that no pre-steaming and no separate impregnation step were performed. The experiments were conducted in duplicates, and each sample was cooked for 4 h whilst mounted on the sample stage and monitored with X-ray CT. During cooking, the temperature inside the reactor varied between 135 and 150 °C, as the liquor circulation was stopped every time the reactor was exposed to the X-ray beam. A summary of the experimental conditions utilized for the tests is given in Table 1.

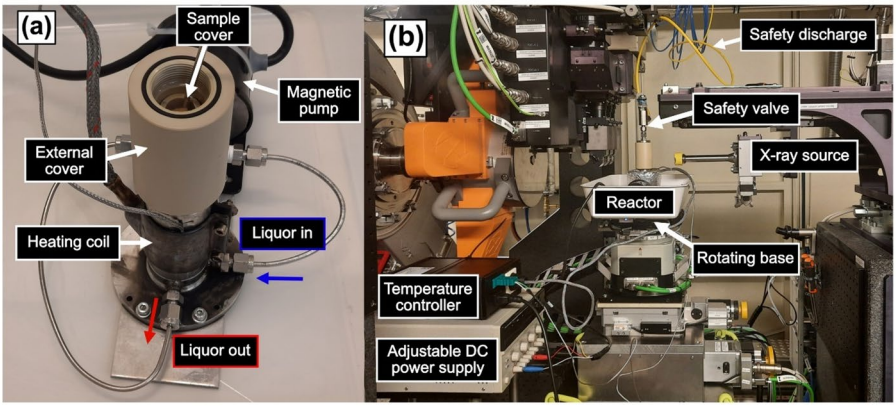

Fig. 2 Reactor: **a** open cell highlighting the main components and the path of liquor circulation, **b** picture of the reactor mounted at the ForMAX beamline

Table 1 Cooking conditions and white liquor composition

Parameter	Value
Temperature (set point, °C)	141
[HO^-] (mol/kg liquor)	0.55
[HS^-] (mol/kg liquor)	0.25
Na_2CO_3 (mol/kg liquor)	0.10
Liquor: wood (w: w) [a]	Approx. 90:1

[a] High liquor-to-wood ratio was used due to the reactor design and to ensure somewhat constant concentration of cooking chemicals in the bulk liquor

In-situ X-ray tomography

Fifteen local tomography measurements were taken for each sample during the reaction time. The use of local CT meant that the 3D images covered a field-of-view within the sample volume, and the full sample cross-section was not captured, which enabled higher resolution whilst maintaining a pertinent sample size. The first 7 measurements were spaced by 10 min, whereas the last 8 were performed every 15 min (to minimize radiation damage). During image acquisition, the liquor circulation inside the reactor was stopped to minimize motion artefacts and noise.

The beam energy was 22.5 keV and the detection system included a 10× zoom optical microscope (Optique Peter) reaching an effective pixel size of 0.65×0.65 µm^2 with a sCMOS camera (Andor Zyla 5.5). The nominal field-of-view was 1.1 mm x 0.7 mm^2 and the scanned volumes corresponded to the middle portion of the chips (Fig. 1). In addition, all the scans were performed over a 180° rotation of the stage with a total of 1800 projections acquired over 18 s (with increments of 0.1° and 10 ms of exposure time). More details about the beamline and its experimental station are described by Nygård et al. (2024).

Image reconstruction and analysis

Image reconstruction was carried out using the Gridrec algorithm (Dowd et al. 1999; Rivers 2012) implemented via *TomoPy* (Gürsoy et al. 2014). Prior to tomographic reconstruction, phase retrieval was performed on the radiographic projections ($\alpha_{regularization} = 0.001$ and sample to detector distance of 1 cm). After the reconstruction it was noticed that the position of the samples shifted slightly between the first scanned image (time = 0 min) and the subsequent 14, likely due to the penetration of the liquor. Hence, to allow a better comparison of the tomograms, the reconstructed images were registered spatially and re-aligned using zero-normalized correlation routines (see the Supplementary Information). Gaussian filtering was also applied to minimize noise (sigma values: x = y = 15, z = 5). One example of a 2D slice of a reconstructed tomogram can be seen in Fig. 3a.

Further image processing was conducted using ImageJ-*Fiji* (Schindelin et al. 2012). Image segmentation (binarization) was performed with the *Trainable Weka Segmentation* ImageJ-plugin (Arganda-Carreras et al. 2017), by creating a classifier based on two classes, pores and cell walls, and applying the default settings for training. The segmented (binary) images were corrected by removing unconnected regions utilizing the *Interactive Morphological Reconstruction 3D* tool in the *Mor-*

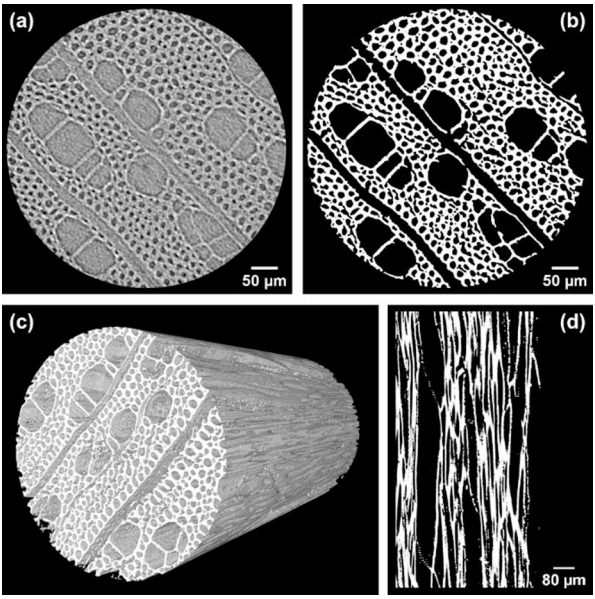

Fig. 3 Example of image reconstruction and segmentation: **a** 2D transverse slice of the reconstructed tomogram, **b** same 2D transverse slice after segmentation, **c** 3D segmented image from which the 2D slice was taken, and **d** tangential view of the segmented volume. All images were taken from a birch sample after 57 min of pulping

phoLibJ plugin (Legland et al. 2016), utilizing reconstruction by dilation and connectivity = 6. Segmented images of tomograms collected before cell wall separation were also corrected by using the *Remove Outliers* tool, selecting the radius according to visual inspection. One example of a segmented 3D image and some of its 2D slices are shown in Fig. 3b-d.

The porosity of each sample was computed from the 3D segmented (binarized) images based on the percentage of 0-value (dark) voxels within the binary volume. Prior to the full data analysis, preliminary tests involving the comparison of porosities estimated from different trainings of the Weka algorithm were used to estimate the error associated with the binarization process. These tests were conducted by segmenting one reconstructed 3D image using different classifiers and then determining the residual standard deviation among the porosities of the resulting binary images. According to this analysis, the binarization error was estimated to be about 5% with respect to the computed global porosity values.

3D binary images were also used to measure the average values of cell wall thickness and lumen size. These averages were determined using the *Local Thickness* plugin (Dougherty and Kunzelmann 2007), which evaluates the diameter of the largest sphere that fits inside the object defined by non-zero voxels at a given point. Thus, when calculating the averages of cell wall thickness, no distinction was made between the different cells, as all of them were classified under the same label. Moreover, the results were expressed as either double wall thickness, measured between two lumens before cell wall separation, or single wall (measured after cell wall separation). To determine the average lumen size, the binary segmented images were inverted before performing the local thickness analysis and a threshold was applied to the result to exclude vessels.

The separation of cell walls was also investigated by comparing the grayscale levels in different reconstructed images. This comparison was conducted by subtracting a reference (image taken after complete liquor penetration) from the image under analysis (e.g., image taken after significant delignification) and applying the segmented image of the reference as a mask. Before subtraction, the consecutive images were re-aligned locally by registering smaller sub-volumes within the sample. Furthermore, the spatial evolution of gray levels within the cell wall and middle lamella was investigated. This analysis was carried out by creating a distance field based on the segmented reference (mask) and then using it as a label to compute the local averages of grayscale levels in the consecutive reconstructed images. The distance field was created using *Chamfer Distance Map 3D*, and the local averages were calculated using *Intensity Measurements 2D/3D*, which are both tools available in the *MorphoLibJ* plugin. Refer to the Supplementary Information for more details about these steps.

Optical microscopy

Optical micrographs of untreated wood were acquired to provide a basis of comparison for the images attained via *in-situ* CT (at pulping time = 0 min). To prepare the slides used in the microscopy analysis, air-dried sapwood chips of the three hardwoods under study were softened in deionized water. The small pieces (~ 1.5 cm x 8 mm x 8 mm) were first soaked for 10 min in water with the aid of a vacuum chamber and then heated (approx. 80 °C / 1–2 h) under constant agitation. Transverse sections (thickness = 100–150 μm) of the softened samples were produced with the aid of a microtome (Jung AG, Heidelberg). These sections were mounted in microscope slides using deionized water as mounting medium and covered with coverslips. The slides were observed with a light microscope (Axio Imager Z2m, Zeiss) in bright-field mode with a maximal magnification of 400x. Image processing was performed with ImageJ-*Fiji*, using an approach similar to the one described in Sect. 2.4 (i.e., image segmentation followed by *Local Thickness* analysis).

Lignin and carbohydrates analysis

In order to assess the extent of delignification achieved after subjecting sapwood chips to the pulping conditions utilized in the beamline, wood and pulp samples were analyzed to determine the contents of Klason lignin and carbohydrates. The pulp samples were prepared in a lab, using the same reactor and the same cooking conditions utilized in the *in-situ* experiments (Table 1), including the intervals in which the pump was shutdown. Then, both sapwood and pulp samples were subjected to acidic hydrolysis, using a procedure based on the NREL's method for determination of structural carbohydrates and lignin (Sluiter et al. 2012). A detailed description of the procedure is given in previous work (Marion de Godoy et al. 2024).

To measure Klason lignin, the hydrolysate was filtered in glass microfiber filters (Whatman GF/A), and the solid residue was dried at 105 °C overnight and weighed. The filtrate was used to quantify the carbohydrates using anion exchange chromatography (HPAEC-PAD Dionex ICS-5000, Thermo Fisher Scientific). Separation was

carried out with two 250 mm Dionex CarboPac PA1 columns, and detection was done with a pulsed amperometric detector equipped with a gold reference electrode. The results were corrected by the yields of hydrolysis, as reported by Wojtasz-Mucha et al. (2017). The final concentrations of carbohydrates were expressed as anhydro sugars.

Estimate of porosity based on density

The porosity calculated via tomography (pulping time = 0 min) was compared to the porosity of untreated sapwood samples calculated based on density measurements. Initially, the density values (in dry basis) were determined by measuring the oven-dried mass of wood pieces with specific dimensions and then dividing the results by the volume of said pieces. The density was used to calculate the porosity according to Eqs. 1,

$$\epsilon_i = 1 - \frac{\rho_i}{\rho_w} \tag{1}$$

where ϵ_i is the porosity of the wood sample, ρ_i is the density of the wood sample in dry basis, and ρ_w is the density of the wood substance. The value of ρ_w was set to 1500 kg/m^3, which is an approximate value (Malkov et al. 2001a).

Results and discussion

Microstructure of untreated hardwoods and assessment of reconstructed tomograms

The microstructures of the three hardwoods under study (untreated samples, pulping time = 0 min) are shown in Fig. 4. The first images (Fig. 4a-c) display 2D slices of the reconstructed tomograms, in which it is possible to observe some of the anatomical differences between the species, like the presence of slightly smaller vessels in alder (Fig. 4a) and slightly thicker rays in birch (Fig. 4c). The quality of the reconstructed tomograms was on par with the results achieved by Wagih et al. (2022). The spatial resolution and voxel contrast of the images is limited due to inherent external interference present in the system and the pronounced local tomography. With these limitations, smaller features, such as pits (~1–2 μm), could not be properly detected in the samples.

Measurements of morphological data based on the reconstructed tomograms (3D images) were also compared with results attained using micrographs acquired via optical microscopy, e.g., as shown in Fig. 4d-f. Table 2 summarizes this comparison and presents porosity data calculated from the binarized tomograms and based on the density measurements.

Overall, the results shown in Table 2 indicate that the reconstructed tomograms provided reasonable measurements of the selected structural features with respect to the more standard measurement approaches. The porosity values reflected microstruc-

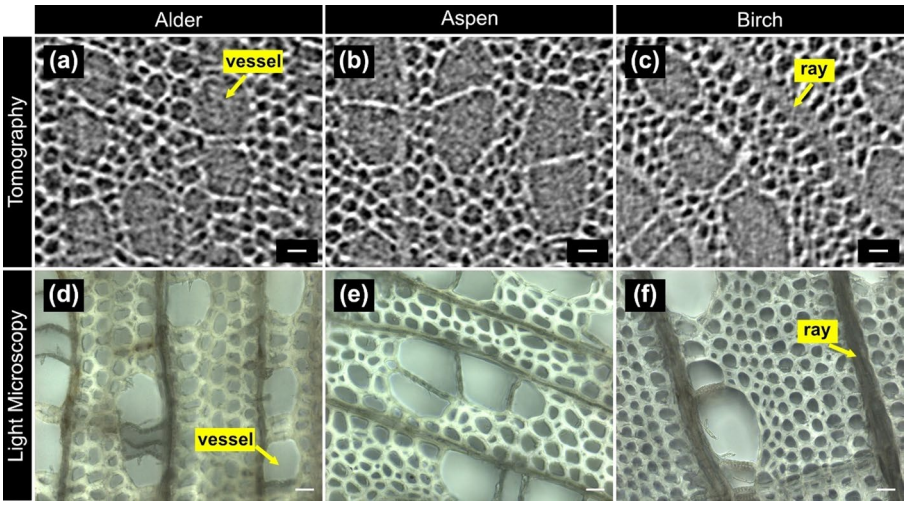

Fig. 4 Microstructure of the hardwoods under study. The grayscale images show 2D transverse slices of the reconstructed tomograms acquired in the beginning of the experiments (pulping time = 0 min) for **a** alder, **b** aspen, and **c** birch. The images in the second row show transverse slices of **d** alder, **e** aspen, and **f** birch observed with light microscope. Scale bars = 20 µm

Table 2 Porosity, double wall thickness, and lumen diameter (of fibers) in different hardwood species

	Alder (*A. glutinosa*)	Aspen (*P. tremula*)	Birch (*B. pubescens*)
Porosity (%)			
via tomography [a]	65.4 ± 3.3	68.5 ± 3.4	56.6 ± 2.8
based on density [b]	66.7 ± 1.0	71.5 ± 1.8	61.7 ± 0.0
Double wall thickness (µm) [c]			
via tomography	7.1 ± 1.8	7.2 ± 1.9	7.4 ± 1.7
via microscopy	6.5 ± 2.5	6.6 ± 2.3	7.1 ± 2.3
Lumen diameter (µm) [c]			
via tomography	13.9 ± 5.0	13.0 ± 4.6	9.9 ± 3.1
via microscopy	12.7 ± 4.0	11.4 ± 3.4	11.5 ± 2.7

[a] The standard deviations were calculated considering the estimated error of the segmentation procedure (5%)

[b] Porosity estimated based on density measurements of oven-dried wood chips and considering the density of the wood substance = 1500 kg/m^3

[c] The averages and standard deviations were calculated based on the histograms of the measurements conducted in the segmented images

tural differences between the hardwood species, especially the size and frequency of vessels, as other important factors such as cell wall thickness and the lumen diameter of fibers appear to be similar among the samples. Moreover, the CT-based porosities of aspen and alder were in good agreement with the data estimated using wood density. A small difference was observed between the porosity values calculated for

birch, which may be due to the small field-of-view used in the tomography experiments. This difference could also be associated with the simplifications performed when estimating the porosity via density, as more accurate results could be achieved if ρ_w was measured or calculated based on the composition of the hardwoods under study.

Regarding double wall thickness and lumen diameter, the results were within the range found in previous works (Kaakinen et al. 2004; Patt et al. 2006; Kiaei et al. 2016; Takata et al. 2021), and no significant differences were observed between the species. However, the standard deviation of the results was substantial, although it likely reflected the intrinsic variations in the wood tissue rather than measurement errors. The large deviations are also explained by the fact that in both the tomography and the microscopy data no distinction was made between the fibers and the other cells in the wood tissue (except for vessels, which were excluded from the lumen measurements).

Liquor penetration in hardwoods during kraft pulping

Figure 5 presents tomogram slices of birch (Fig. 5a-c) and aspen chips (Fig. 5d-f). The images include the first acquired after starting the pulping experiments (Fig. 5a and d), the last before complete liquor penetration (Fig. 5c and f), and some collected

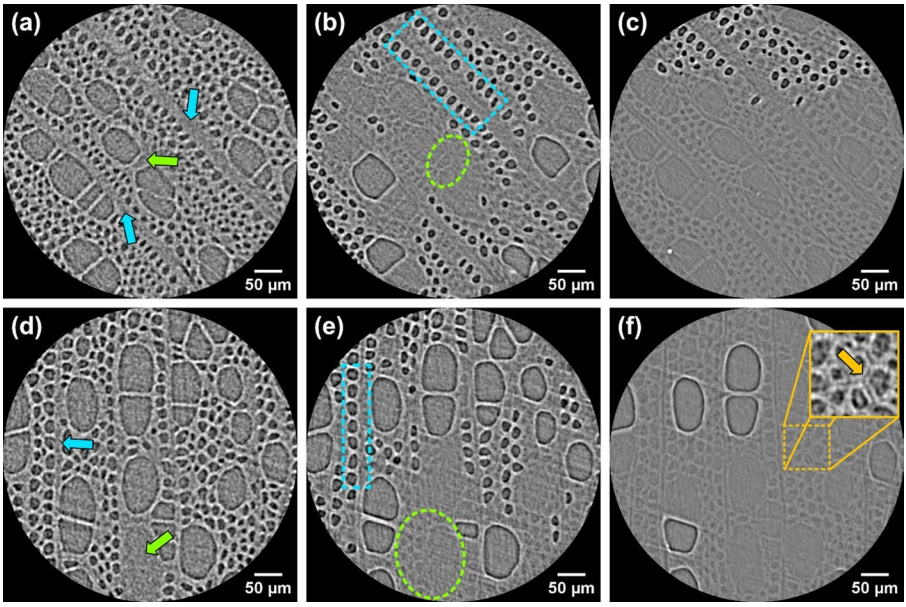

Fig. 5 *In-situ* tomograms following the penetration of cooking liquor in the center of wood chips. 2D slices of the reconstructed images of birch **a**–**c** after 15, 29, and 43 min of pulping. 2D slices of the reconstructed images of aspen (d)-(f) after 24, 39, and 67 min of pulping. The regions with lower contrast correspond to the areas filled with liquor. In images **a** and **d**, the blue and green arrows indicate, respectively, some of the first rays and vessels to be filled. Similarly, in images **b** and **e** the highlighted areas in blue and green indicate the lumens of the fibers adjacent to a ray cell (rectangles) and a vessel (circles). The magnified area in **f** shows the beginning of cell wall separation in aspen

in between (Fig. 5b and e). Together, they illustrate how the penetration of white liquor progressed inside hardwoods with different porosities.

Although the conditions for liquor penetration in the experiments differed from those found in an industrial setting, they allowed comparing the behavior of the hardwoods when entrapped air is present inside vessels and fibers. More details about the movement of entrapped air within the chips are described in the Supplementary Information.

In both species, the rays were the first cells to be fully penetrated by the cooking liquor, together with a few vessels (refer to the arrows in Fig. 5a and d). This result is consistent with expectations, as the thickness and width of the samples were considerably smaller than their length, and the region under study was located in the center of the chips. The result also reinforces previous findings (Wardrop and Davies 1961; Ahmed and Chun 2011) that indicate that ray cells offer a path for radial transport of liquor, while vessels offer the main path for penetration in the longitudinal direction of hardwoods.

In addition to identifying which cells were penetrated first by the liquor, it is interesting to observe how the liquor is transported to the lumen of the fibers. It was shown by Stone and Green (1959) that longitudinal penetration of liquor from fiber to fiber is not an efficient path of impregnation and, instead, the penetration of liquor in the lumens occurs from an impregnated cell to the adjacent ones via the pit system. In this context, the tomograms presented in Fig. 5b and e suggest that liquor penetration from ray cells to adjacent fibers is not as fast or efficient as the penetration starting from vessels. This phenomenon can clearly be observed by comparing the highlighted areas in blue and green in Fig. 5b and e: the lumen of the fibers close to the rays (blue rectangles) is empty, whereas the fibers close to vessels (green circles) are filled with liquor. This behavior could be explained by the differences in number, size, and type of pits in these cells. For instance, the pits in ray cells are relatively small compared to the pits in vessels (Carlquist 2007; Ahmed and Chun 2011), which may slow down the passage of liquor to the adjacent fibers. Moreover, differences in the thickness and porosity of pit membranes have also been suggested to affect the uniformity of impregnation (Singh et al. 1999).

Nevertheless, despite providing a poor pathway for cross penetration, the rays still contribute to the transport of cooking chemicals via diffusion through the cell walls. In addition, they may play an important role in the distribution of cooking chemicals in the middle lamella, as the percentage of blind pits (i.e., pits connecting the rays to extracellular spaces) can be quite significant in some wood species (Zhang et al. 2004).

The tomograms in Fig. 5c and f show the profile of the samples just before being completely filled with liquor. The fibers were the last features to be filled in birch, whereas in aspen some vessels were still empty after all fibers were penetrated. Such a difference is probably related to the porosity of the samples. The aspen sample had a larger porosity than birch, which most likely extended the time for complete liquor penetration in the sample, as more liquor had to be transported in and more entrapped air had to be transported out. This hypothesis is reinforced by the results obtained for the alder sample, which also had a larger porosity than birch. In this case, images of liquor penetration reveal that alder behaved like aspen, i.e., the fibers were

completely filled with liquor while some vessels still had air inside them (refer to the Supplementary Information). Nonetheless, despite the longer times required for complete liquor penetration in aspen and alder, the delignification of the fibers did not seem to be significantly delayed. In fact, the aspen samples even displayed the beginning of cell wall separation before all vessels were filled with liquor, as shown by the dark lines along the middle lamella in the magnified area of Fig. 5f.

When comparing the behavior of liquor penetration in this study with the liquor penetration in more fractured wood chips, like those prepared in industrial chippers, one can anticipate differences. Based on early impregnation experiments (Gustafson et al. 1989), most of the differences between liquor penetration in hand-cut chips and commercial ones are associated with the rate of penetration. Nevertheless, the mode of penetration, i.e., the transport of liquor between adjacent cells via pits, should remain the same. Similarly, when comparing the behavior of liquor penetration with and without the presence of entrapped air, changes in the rate of penetration should be expected, as the air can create significant back pressure. Still, this effect should be more pronounced in heartwood than sapwood (Malkov et al. 2001b).

Progression of delignification inside hardwoods during kraft pulping

Table 3 presents the times required to achieve complete liquor penetration and fiber separation in the center of the hardwood chips, according to visual inspection of the reconstructed images acquired via *in-situ* CT. Additionally, Table 3 shows the changes in composition (specifically Klason lignin, glucan, and xylan) measured in hardwood chips treated using the same pulping conditions applied in the *in-situ* experiments.

The compositional analysis showed that the initial lignin concentration in alder was substantially higher than in the other species (by approx. 28%), whereas birch

Table 3 Progression of kraft pulping in different hardwood chips

	Alder (*A. glutinosa*)	Aspen (*P. tremula*)	Birch (*B. pubescens*)
Composition [a] (%, odw)			
Before pulping (0 h)			
Klason lignin	24.9±0.4	19.6±0.6	19.3±0.4
Glucan	40.0±0.6	43.0±0.8	37.0±0.2
Xylan	17.6±0.2	16.5±0.3	23.2±0.2
After pulping (4 h)			
Klason lignin	1.1±0.4	0.4±0.1	0.6±0.0
Glucan	30.1±0.0	30.8±0.0	33.4±0.1
Xylan	6.0±0.2	4.7±0.1	7.5±0.1
Pulping stage [b]			
Complete liquor penetration (h)	1.4	1.4	1.0
Start of cell wall separation (h)	1.6	1.1	1.4
Complete separation of fibers (h)	2.9–3.2	2.2–2.5	2.3–2.7

[a] Results expressed in weight% of dry wood. Minor components, like other hemicellulose-related sugars, extractives, and ash, were omitted. The following pulping yields were measured for the samples after 4 h of pulping: 40% for alder, 39% for aspen and 44% for birch.

[b] Based on visual inspection of the reconstructed tomograms. Note that the terms "cell wall separation" and "fiber separation" are used interchangeably in this text

had the largest amount of xylan and aspen the highest content of glucan. After pulping, more than 95% of the initial lignin was removed from all the samples, indicating that the 4 h experiments were sufficient to capture the overall delignification profile of all wood species.

The data regarding complete liquor penetration and cell wall separation highlighted differences between the three wood species. As discussed in Sect. 3.2, liquor penetration was likely affected by the porosity of the samples and progressed slightly faster in birch (the least porous material). Cell wall separation, which is a direct result of lignin removal, can be influenced by many factors, ranging from local lignin content and composition (Santos et al. 2011; Aguayo et al. 2014; Takada et al. 2016, 2021) to the availability of alkali and the rates of diffusion of lignin fragments through the fiber walls (Brännvall 2018; Kron et al. 2025). Based on the CT data, the rate of separation seem to agree with the initial content of lignin in the samples and their porosity (which impacts the availability of cooking chemicals within the chip). Aspen was the species in which cell wall separation was detected first and it was also the species with the highest porosity and a somewhat low lignin content. Birch, despite the low lignin content, experienced fiber separation later than aspen. This behavior was probably influenced by the low porosity, as a lower concentration of cooking chemicals should be available in the middle of the birch chip when compared to aspen, especially in the beginning of pulping (i.e., right after liquor penetration). Finally, alder was the last species to go through fiber separation, which was expected given its significantly higher initial lignin content.

The evolution of fiber separation across the microstructure of the samples is examined in more detail in Fig. 6. These results were assessed with reconstructed CT images of birch samples, but similar behavior was observed in aspen and alder (refer to Supplementary Information). In Fig. 6a it is possible to follow the decrease in grayscale levels between the fibers through time. The first image acquired after complete liquor penetration (1.2 h of pulping) showed initial signs of material loss in the middle lamella, as indicated by the decrease in gray values along the boundary between two adjacent fibers. After 1.4 h of pulping, the initial signs of material loss also became visible in the cell corners. Next, as delignification progressed, the material loss in the previously affected regions was intensified, effectively creating a new interface between fiber wall and liquor. At 2.0 h of pulping, cell wall separation was accomplished for most fibers.

The qualitative analysis of grayscale levels shown in Fig. 6a was made quantitative and extrapolated to the whole reconstructed volume in the graph presented in Fig. 6b. The graph showed a continuous decline in gray-levels close to the limits between two adjacent cells, as indicated by the profiles measured at distances equal or above half of the average double wall thickness. Such decline was associated with the decrease in density in the middle lamella region, as the extent of lignin removal increased, and with the formation of a new wall-liquor interface, as fiber separation progressed. The analysis of the behavior close to the lumen, however, is more complex. The gray-levels in this region increased, although the changes were less pronounced than the ones in the interface between cells. This increase probably reflected changes in phase-contrast due to the new interfaces between wall and liquor. Other factors influencing the gray-levels could be related to changes in the secondary

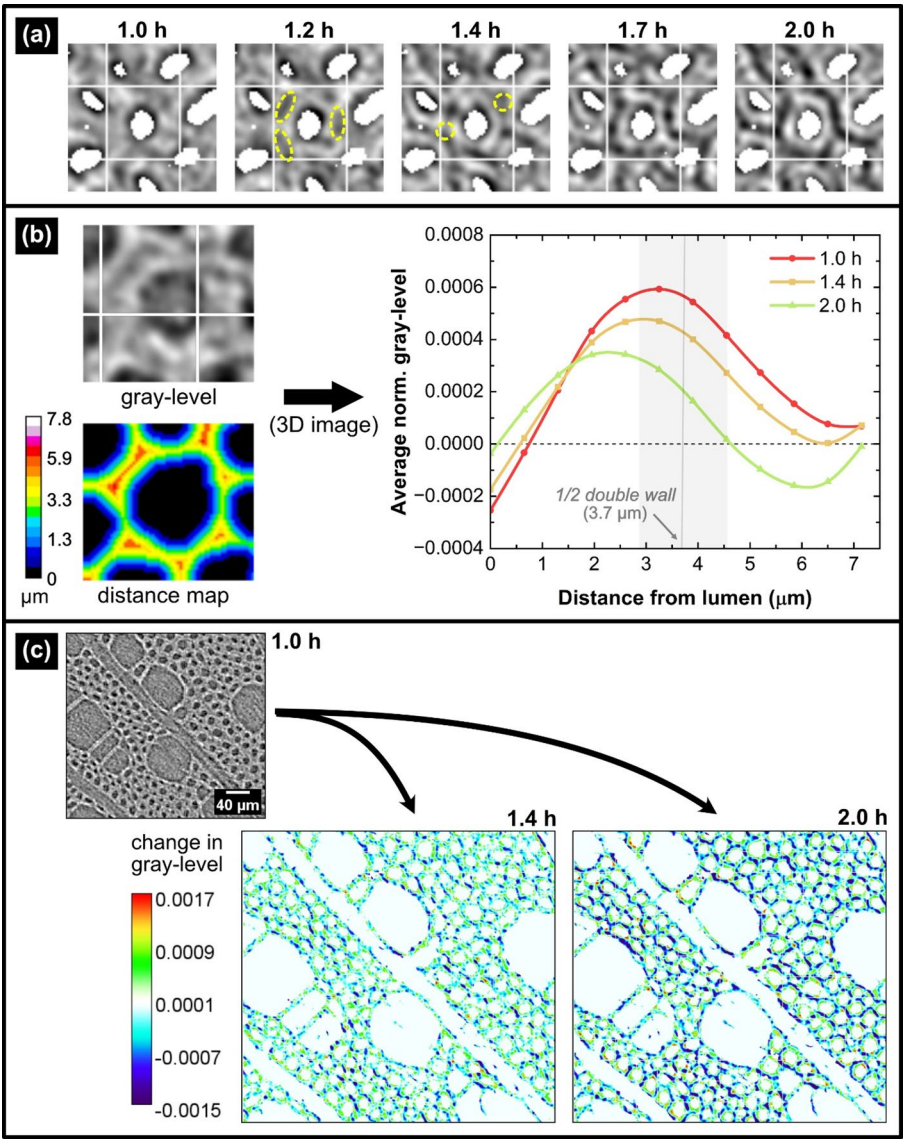

Fig. 6 Delignification and cell wall separation in birch. **a** Zoomed-in reconstructed 2D slices acquired at different pulping times illustrating fiber separation. The areas highlighted in yellow show the initial material loss in the middle lamella (after 1.2 h of pulping) and cell corners (after 1.4 h of pulping). **b** Average spatial variation in grayscale levels across the cell walls and middle lamella of the reconstructed volumes. The vertical line at 3.7 µm indicates half of the average double wall thickness in untreated birch. Max. standard deviation of gray-level = 0.0006 (dimensionless). **c** Maps showing the uniformity of changes in grayscale levels across transverse slices of reconstructed tomograms. Reference: slice acquired after 1.0 h of pulping. On the left: sample after 1.4 h of pulping, on the right: sample after 2.0 h of pulping

wall, as it experiences relatively fast removal of lignin and hemicelluloses followed by aggregation of cellulose fibrils (Hult et al. 2001; Bardage et al. 2004). In addition, after fiber separation the variations in gray-levels may also originate from small movements of the fibers beyond the mask used in the analysis.

In Fig. 6c, changes in grayscale levels across the microstructure were measured to provide an indication of the uniformity of delignification in the transverse section of wood and the potential impact of different cells in the progression of fiber separation. This measurement was conducted by subtracting the gray-levels of a reference (reconstructed slice acquired at 1.0 h of pulping) from re-aligned reconstructed slices acquired at 1.4 h and 2.0 h of pulping. The resulting maps suggest a seemingly homogenous extent of delignification along the transverse slices, as indicated by similar gray-level changes in the boundary of adjacent fibers spread across the monitored area. Thus, the position of a fiber relative to other cells did not appear to affect the rate of lignin removal substantially, i.e., being in the vicinity of a vessel or a ray cell led to neither speeding-up nor slowing-down of the delignification process (considering the sensitivity limits of the gray-scale analysis).

The progression of pulping was also described by changes in the porosity of the samples and changes in the double/single wall thickness, as presented in Fig. 7. Due to the differences in contrast between regions filled with liquor and those filled with air, segmentation and subsequent measurements in the reconstructed CT images with partial liquor penetration were not possible. Hence, the profiles in Fig. 7 show results acquired before pulping (time = 0 h) and after complete liquor penetration.

The overall increase in porosity with cooking time was an expected trend. In the samples observed before and after liquor penetration there were no significant variations in porosity, as the only changes seen in the tomograms referred to minor expansions in the thickness of the rays (see measurements in the Supplementary Information). The only exception occurred in aspen, as cell wall separation had already started during liquor penetration. As pulping progressed, the porosity of the samples increased due to the separation of fibers and, later, due to further distancing of the cells. Among the hardwoods, birch had the largest increase in porosity (from 56.6% to 75.7%, i.e., 33.7%), which was also anticipated since birch had the highest ratio between fibers and vessels.

Regarding the evolution of the double/single wall thickness (Fig. 7b), it is interesting to note the differences between the profiles found in this study and the ones found by Wagih et al. (2022) in their *in-situ* experiments. When working with soda pulping, Wagih et al. (2022) observed that the double wall thickness in compression wood of Norway spruce increased by more than 60% within the first 10 min of process. This expansion remained significant even after the first hour of pulping, as the double wall was still approximately 16% larger than in the untreated wood. In the current study, however, the measurements of double wall thickness in the hardwoods before and after liquor penetration did not suggest a substantial expansion of the wall. In addition, visual inspection of the images collected during liquor penetration (i.e., between 0 and 1 h of pulping) also pointed at a relatively constant fiber wall thickness. This difference suggests how the fiber wall ultrastructure could affect the swelling of the lignocellulosic matrix. For instance, in regular wood (as the samples investigated in this study) the almost perpendicular alignment of the cellulose fibrils between the S1,

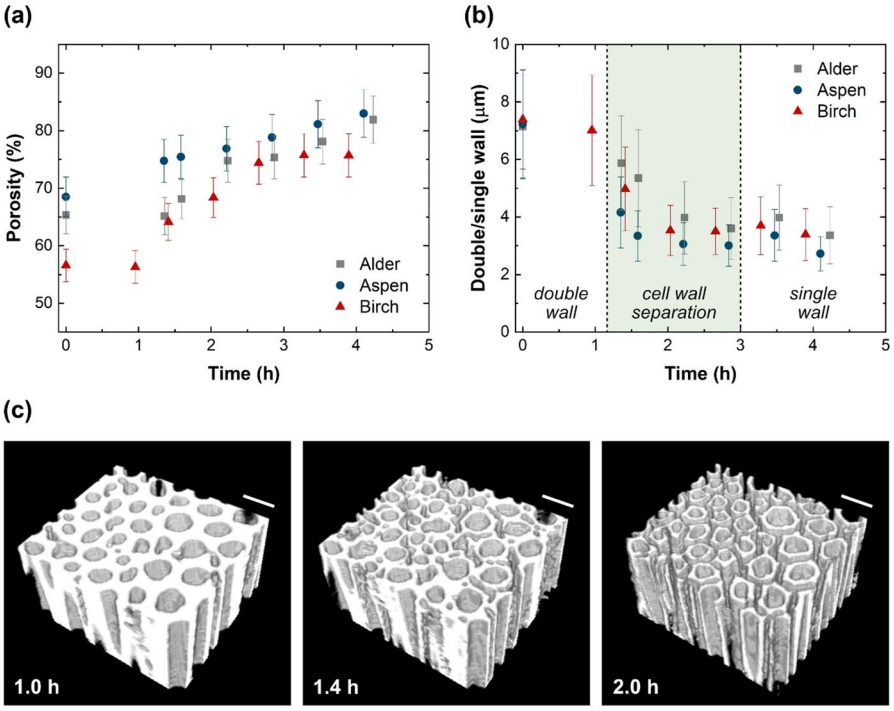

Fig. 7 Evolution of **a** porosity and **b** cell wall thickness in the center of different hardwoods throughout kraft pulping. The area highlighted in green denotes the time interval in which fiber separation is happening. **c** Reconstructed and segmented images of birch illustrating the separation of fibers; from left to right: sample after complete liquor penetration (1.0 h of pulping), sample in the initial stage of fiber separation (after 1.4 h of pulping), and sample with most fibers completely separated (after 2.0 h of pulping). Scale bar = 20 µm

S2 and S3 layers likely restricted the swelling of the S2 layer, which is the thickest and, therefore, the one expected to swell the most (Hubbe et al. 2024). Hence, as the liquor occupied the macropores formed by the removal of lignin and hemicelluloses, the swelling was confined by the secondary wall layers (Stone and Scallan 1967), resulting in minor increase in cell wall thickness. In compression wood, however, the S3 layer is often missing and the microfibril angles in the S2 and S1 layers differ from those found in regular wood (Donaldson and Singh 2013). The cell wall is also thicker and more rounded. These circumstances may allow the wall to expand towards the lumen area during swelling, resulting in a more substantial increase of cell wall thickness.

After complete liquor penetration, the profiles shown in Fig. 7b indicate a sharp decrease in cell wall thickness, as the measurements change from double wall to single wall, reflecting the separation of the fibers. In all samples, this separation was achieved within 1–1.5 h (i.e., after about 2–2.5 h of pulping), as illustrated by the segmented images of birch in Fig. 7c. During the last hour of pulping, no significant changes in cell wall thickness were observed in the samples. Moreover, in birch and alder the final single wall thickness was about 6–8% smaller than half of the double

wall in the untreated wood (Table 2), whereas in aspen this reduction reached 25%. This decrease in thickness agrees with the behavior expected during kraft pulping and likely reflects both the dissolution of the middle lamella and the shrinkage of the secondary wall. However, Stone and Scallan (1967) suggested a gradual decrease in cell wall thickness as the pulping yields become lower than 70%, which was not observed in the profiles of Fig. 7b, although the error bars of the measurements may overshadow such a continuous decline. In addition, the data presented by Stone and Scallan (1967) showed about 20% reduction in cell wall volume in spruce fibers pulped up to 40% yield, which aligns with the results attained with aspen but differs from the modest 6–8% reduction shown in birch and alder. This suggests that the shrinkage of the cell wall may vary from species to species. One can suppose that the small reduction of cell wall thickness in alder and birch may be connected to their high contents of residual xylan (when compared to aspen), but further research into the evolution of cell wall density and cellulose fibril aggregation during pulping of hardwoods is needed to assess this hypothesis.

Final discussion

In-situ X-ray tomography was successfully applied to observe changes in the structure of three hardwood species during kraft pulping. The 3D reconstructed tomograms allowed measurement of morphological features, namely cell wall thickness and lumen diameter, of alder, aspen and birch samples, with results comparable to the ones achieved using optical microscopy and other imaging techniques. Moreover, the *in-situ* experiments allowed the structures and their evolution to be followed in 3D during pulping to provide information on liquor penetration and delignification of the wood chips. Liquor penetration was shown to start in vessels and ray cells, confirming results from earlier works (Stone and Green 1959; Wardrop and Davies 1961). The images also indicated that the preferred path for the propagation of liquor penetration in adjacent cells began in vessels rather than in rays, likely due to the size and configuration of the pits. Hence, future work comparing the pitting system in rays and vessels and their structural changes when exposed to alkaline medium may be relevant to elucidate the details of liquor penetration during kraft pulping and to explain differences in the impregnability of different wood species.

For the hardwoods evaluated in this study, no significant differences were observed regarding the route of liquor penetration. However, the total time required for complete penetration varied, with the most porous hardwoods (aspen and alder) taking longer to be filled by liquor. In addition, the samples showed different delignification rates, as evidenced by the pulping times needed to achieve complete fiber separation. Aspen was the fastest to delignify, whereas alder took the longest time until fiber separation. The reasons for these differences in pulpability are still not fully understood, but the porosity of the material and its initial lignin content are suggested to influence the process significantly.

The reconstructed tomograms also revealed that the extent of lignin removal was not influenced significantly by the radial or angular position of the fibers relative to other cells. Furthermore, delignification was shown to affect the middle lamella from

the early stages of pulping, as observed by changes in grayscale levels of images acquired after complete liquor penetration.

Measurements of porosity and double wall thickness during pulping indicated that the most drastic structural changes in all samples happened within 1–1.5 h after complete liquor penetration. At the end of the pulping experiments, the hardwoods presented a 21–34% increase in porosity caused by fiber separation and further distancing of the cells due to slight movement of the fibers and cell wall shrinkage. The lack of a pronounced increase in double wall thickness during the beginning of pulping highlighted the impact of the cell wall ultrastructure in restraining the swelling of the lignocellulosic matrix. Moreover, the results attained after substantial delignification suggested differences in the intensity of fiber wall shrinkage in the different wood species.

Conclusion

The present study showed how *in-situ* X-ray microtomography can be applied to investigate liquor penetration and delignification during kraft pulping. The reconstructed images of different hardwood species during cooking indicated that:

- Vessels provide the best path for liquor penetration, allowing it to be transported to adjacent cells via pit pores. Ray cells, on the other hand, become filled with liquor relatively quickly but do not allow easy passage of liquor to the surrounding fibers.
- Fiber separation starts earlier in aspen, then in birch and later in alder.
- The proximity of fibers to vessels and ray cells does not impact the rate of fiber separation significantly.
- Cell wall thickness decreases during pulping, which reflects the loss of the middle lamella and the shrinkage of the secondary wall. The extent of the decrease varies between species.
- The wood chip porosity increases continuously due to cell wall separation and, after extensive delignification, due to cell wall shrinkage and small movements of the fibers.

Supplementary Information The online version contains supplementary material available at https://doi.org/10.1007/s00226-026-01767-6.

Acknowledgements We acknowledge the MAX IV Laboratory for beamtime on the ForMAX beamline under proposal 20240397. Research conducted at MAX IV, a Swedish national user facility, is supported by Vetenskapsrådet (Swedish Research Council, VR) under contract 2018-07152, Vinnova (Swedish Governmental Agency for Innovation Systems) under contract 2018-04969 and Formas under contract 2019-02496. The authors would like to thank Dr. Mira Viljanen (MAX IV) for her support during the experiment at ForMAX, as well as Södra Skogsägarna for supplying the raw materials used in this study. Finally, the collaboration and financial support of the Resource-smart Processes Graduate School, financed by Vinnova via BioInnovation and industrial partners (Billerud, Holmen, SCA, Stora Enso, Södra Skogsägarna, and Valmet), is gratefully acknowledged.

Author contributions Study conception and design: Carolina Marion de Godoy, Stephen A. Hall, Merima Hasani, and Hans Theliander. Material preparation and data collection: Carolina Marion de Godoy, Klara

Hackenstrass, Luigi Galluccio, Endri Laçaj, Haiyang Yu, Sara Florisson, Malin Wohlert, and Stephen A. Hall. Data analysis: Carolina Marion de Godoy and Endri Laçaj. Interpretation of results: All authors contributed to the interpretation of the results. The first draft of the manuscript was written by Carolina Marion de Godoy and all authors commented on previous versions of the manuscript. All authors read and approved the final manuscript.

Funding Open access funding provided by Chalmers University of Technology. This work was performed within the strategical innovation program BioInnovation - a joint initiative by Vinnova (Sweden's innovation agency), Formas (a Swedish research council for sustainable development), and the Swedish Energy Agency. Sara Florisson was supported by the Swedish Research Council (Vetenskapsrådet, VR) via Grant 2023–04705. Likewise, Endri Laçaj and Stephen Hall were supported by the VR funded STIMULI project (#2022–06049).

Data availability The raw data files are available upon reasonable request from the corresponding author.

Declarations

Conflict of interest The authors have no competing interests to declare that are relevant to the content of this article.

References

Aguayo M, Ferraz A, Elissetche J, Masarin F, Mendonça R (2014) Lignin chemistry and topochemistry during kraft delignification of *Eucalyptus globulus* genotypes with contrasting pulpwood characteristics. Holzforschung 68:623–629. https://doi.org/10.1515/hf-2013-0190

Ahmed SA, Chun SK (2011) Permeability of *Tectona grandis* L. as affected by wood structure. Wood Sci Technol 45:487–500. https://doi.org/10.1007/s00226-010-0335-5

Arganda-Carreras I, Kaynig V, Rueden C, Eliceiri KW, Schindelin J, Cardona A, Sebastian Seung H (2017) Trainable Weka Segmentation: a machine learning tool for microscopy pixel classification. Bioinformatics 33:2424–2426. https://doi.org/10.1093/bioinformatics/btx180

Bacarin GB, Cabrera FC, da Silva MR, Job AE (2017) The distribution of Lignin and Xylan in the Inner and Surface Layers of the Fiber from Eucalyptus Kraft Pulp and its Effects on Oxygen Delignification. Mat Res 20:945–950. https://doi.org/10.1590/1980-5373-MR-2016-0687

Bardage S, Donaldson L, Tokoh C, Daniel G (2004) Ultrastructure of the cell wall of unbeaten Norway spruce pulp fibre surfaces. Nord Pulp Pap Res J 19:448–452. https://doi.org/10.3183/npprj-2004-19-04-p448-452

Biziks V, Van Acker J, Militz H, Grinins J, Van den Bulcke J (2019) Density and density profile changes in birch and spruce caused by thermo–hydro treatment measured by X–ray computed tomography. Wood Sci Technol 53:491–504. https://doi.org/10.1007/s00226-018-1070-6

Brännvall E (2018) Increasing pulp yield in kraft cooking of softwoods by high initial effective alkali concentration (HIEAC) during impregnation leading to decreasing secondary peeling. cellulose Holzforschung 72:819–827. https://doi.org/10.1515/hf-2018-0011

Carlquist S (2007) Bordered pits in ray cells and axial parenchyma: the histology of conduction, storage, and strength in living wood cells. Bot J Linn Soc 153:157–168. https://doi.org/10.1111/j.1095-8339.2006.00608.x

De Ridder M, Van den Bulcke J, Vansteenkiste D, Van Loo D, Dierick M, Masschaele B, De Witte Y, Mannes D, Lehmann E, Beeckman H, Van Hoorebeke L, Van Acker J (2011) High-resolution proxies for wood density variations in *Terminalia superba*. Ann Botany 107:293–302. https://doi.org/10.1093/aob/mcq224

Donaldson LA (2001) Lignification and lignin topochemistry – an ultrastructural view. Phytochemistry 57:859–873. https://doi.org/10.1016/S0031-9422(01)00049-8

Donaldson LA, Singh AP (2013) Formation and Structure of Compression Wood. In: Fromm J (ed) Cellular Aspects of Wood Formation. Plant Cell Monographs, vol 20. Springer, Berlin, Heidelberg, pp 225–256. https://doi.org/10.1007/978-3-642-36491-4_9

Dougherty R, Kunzelmann K (2007) Computing local thickness of 3D structures with ImageJ. Microsc Microanal 13:1678–1679. https://doi.org/10.1017/S1431927607074430

Dowd BA, Campbell GH, Marr RB, Nagarkar VV, Tipnis SV, Axe L, Siddons DP (1999) Developments in synchrotron x-ray computed microtomography at the national synchrotron light source. Proc SPIE 3772:224–236. https://doi.org/10.1117/12.363725

Fabián-Plesníková I, Neis FA, Augustin AH (2022) X-Ray Computed Tomography for 3D Anatomical Analysis of Resin Ducts. In: Fett-Neto AG (ed) Plant Secondary Metabolism Engineering. Methods in Molecular Biology, vol 2469. Humana, New York, pp 201–218. https://doi.org/10.1007/978-1-0716-2185-1_17

Forsberg F, Mooser R, Arnold M, Hack E, Wyss P (2008) 3D micro-scale deformations of wood in bending: Synchrotron radiation μCT data analyzed with digital volume correlation. J Struct Biol 164:255–262. https://doi.org/10.1016/j.jsb.2008.08.004

Garskaite E, Stoll SL, Forsberg F, Lycksam H, Stankeviciute Z, Kareiva A, Quintana A, Jensen CJ, Liu K, Sandberg D (2021) The Accessibility of the Cell Wall in Scots Pine (*Pinus sylvestris* L.) Sapwood to Colloidal Fe_3O_4 Nanoparticles. ACS Omega 6:21719–21729. https://doi.org/10.1021/acsomega.1c03204

Gullichsen J, Kolehmainen H, Sundqvist H (1992) On the nonuniformity of the kraft cook. Pap Puu 74:486–490

Gürsoy D, De Carlo F, Xiao X, Jacobsen C (2014) Tomopy: a framework for the analysis of synchrotron tomographic data. J Synchrotron Radiat 21:1188–1193. https://doi.org/10.1107/S1600577514013939

Gustafson RR, Jiménez G, McKean WT, Chian D (1989) The role of penetration and diffusion in nonuniform pulping of softwood chips. Tappi J 72:163–167

Hartwig-Nair M, Florisson S, Wohlert M, Gamstedt EK (2024) Characterisation of hygroelastic properties of compression and opposite wood found in branches of Norway spruce. Wood Sci Technol 58:887–906. https://doi.org/10.1007/s00226-024-01548-z

Hu M, Olsson A, Hall S, Seifert T (2022) Fibre directions at a branch–stem junction in Norway spruce: a microscale investigation using X–ray computed tomography. Wood Sci Technol 56:147–169. https://doi.org/10.1007/s00226-021-01353-y

Hubbe MA, Sjöstrand B, Lestelius M, Håkansson H, Swerin A, Henriksson G (2024) Swelling of Cellulosic Fibers in Aqueous Systems: A Review of Chemical and Mechanistic Factors. BioResources 19:6859–6945. https://doi.org/10.15376/biores.19.3.Hubbe

Hult EL, Larsson PT, Iversen T (2001) Cellulose fibril aggregation – an inherent property of kraft pulps. Polymer 42:3309–3314. https://doi.org/10.1016/S0032-3861(00)00774-6

Kaakinen S, Kostiainen K, Ek F, Saranpää P, Kubiske ME, Sober J, Karnosky DF, Vapaavuori E (2004) Stem wood properties of Populus tremuloides, Betula papyrifera and Acer saccharum saplings after 3 years of treatments to elevated carbon dioxide and ozone. Glob Change Biol 10:1513–1525

Kerr AJ, Goring DAI (1975) The role of hemicellulose in the delignification of wood. Can J Chem 53:952–959

Kiaei M, Naji HR, Abdul-Hamid H, Farsi M (2016) Radial variation of fiber dimensions, annual ring width, and wood density from natural and plantation trees of alder (*Alnus glutinosa*) wood. Wood Res 61:55–64

Koch G, Rose B, Patt R, Kordsachia O (2003) Topochemical investigations on delignification of *Picea abies* [L.] Karst. during alkaline sulfite (ASA) and bisulfite pulping by scanning UV microspectrophotometry. Holzforschung 57:611–618. https://doi.org/10.1515/HF.2003.092

Koddenberg T, Militz H (2018) Morphological imaging and quantification of axial xylem tissue in *Fraxinus excelsior* L. through X-ray micro-computed tomography. Micron 111:28–35. https://doi.org/10.1016/j.micron.2018.05.004

Koddenberg T, Zauner M, Militz H (2020) Three-Dimensional Exploration of Soft-Rot Decayed Conifer and Angiosperm Wood by X-Ray Micro-Computed Tomography. Micron 134:102875. https://doi.org/10.1016/j.micron.2020.102875

Kron L, Hasani M, Theliander H (2025) Heterogenous Diffusion and Reaction Model of Kraft Delignification at the Cell Wall Level. Ind Eng Chem Res 64:1497–1507. https://doi.org/10.1021/acs.iecr.4c03900

Legland D, Arganda-Carreras I, Andrey P (2016) MorphoLibJ: integrated library and plugins for mathematical morphology with ImageJ. Bioinformatics 32:3532–3534. https://doi.org/10.1093/bioinformatics/btw413

Mäkinen T, Halonen A, Koivisto J, Alava MJ (2022) Wood compression in four-dimensional *in situ* tomography. Phys Rev Mater 6:L070601. https://doi.org/10.1103/PhysRevMaterials.6.L070601

Malkov S, Tikka P, Gullichsen J (2001a) Towards complete impregnation of wood chips with aqueous solutions, Part 2: Studies on water penetration into softwood chips. Pap Puu 38:468–473

Malkov S, Tikka P, Gullichsen J (2001b) Towards complete impregnation of wood chips with aqueous solutions, Pat 3: Black liquor penetration into pine chips. Pap Puu 83:605–609

Malkov S, Tikka P, Gustafson R, Nuopponen M, Vuorinen T (2003) Towards complete impregnation of wood chips with aqueous solutions, Pat 5: Improving uniformity of kraft displacement batch pulping. Pap Puu 85:215–220

Maloney TC, Paulapuro H (1999) The Formation of Pores in the Cell Wall. J Pulp Pap Sci 25:430–436

Marion de Godoy C, Hasani M, Theliander H (2024) Kraft pulping of model wood chips: local impact of process conditions on hardwood delignification and xylan retention. Holzforschung 78:446–458. https://doi.org/10.1515/hf-2024-0033

Martha R, Adikurnia IK, Van den Bulcke J, Van Acker J, Dekegeleer M, George B, Rahayu IS, Darmawan W, Gérardin P (2025) Investigating sapwood and heartwood density changes of short rotation teak wood after chemical and thermal modification using X-ray computed tomography. Holzforschung 79:340–351. https://doi.org/10.1515/hf-2025-0014

Martin B, Colin J, Casalinho J, Perré P, Rémond R (2023) Thermo-migration of moisture in Norway spruce assessed by *in-situ* micro-tomography. Constr Build Mater 404:133209. https://doi.org/10.1016/j.conbuildmat.2023.133209

Nygård K, McDonald SA, Gonzalez JB et al (2024) ForMAX – a beamline for multiscale and multimodal structural characterization of hierarchical materials. J Synchrotron Rad 31:363–377. https://doi.org/10.1107/S1600577524001048

Patt R, Kordsachia O, Fehr J (2006) European hardwoods versus *Eucalyptus globulus* as a raw material for pulping. Wood Sci Technol 40:39–48. https://doi.org/10.1007/s00226-005-0042-9

Patterson BM, Cordes NL, Henderson K, Xiao X, Chawla N (2018) Data Challenges of In Situ X-Ray Tomography for Materials Discovery and Characterization. In: Lookman T, Eidenbenz S, Alexander F, Barnes C (eds) Materials Discovery and Design. Springer Series in Materials Science, vol 280. Springer, Cham. https://doi.org/10.1007/978-3-319-99465-9_6

Rehbein M, Pereira M, Koch G, Kordsachia O (2010) Topochemical investigation into the delignification of *Eucalyptus globulus* chips during semi-chemical sulfite pulping. Wood Sci Technol 44:435–449. https://doi.org/10.1007/s00226-010-0363-1

Rivers ML (2012) tomoRecon: high-speed tomography reconstruction on workstations using multi-threading. Proc SPIE 8506:169–181. https://doi.org/10.1117/12.930022

Saka S, Goring DAI (1988) The distribution of lignin in white birch wood as determined by bromination with TEM-EDXA. Holzforschung 42:149–153. https://doi.org/10.1515/hfsg.1988.42.3.149

Santos RB, Capanema EA, Balakshin MY, Chang H-M, Jameel H (2011) Effect of hardwoods characteristics on kraft pulping process: Emphasis on lignin structure. BioResources 6:3623–3637

Schindelin J, Arganda-Carreras I, Frise E et al (2012) Fiji: an open-source platform for biological-image analysis. Nat Methods 9:676–682. https://doi.org/10.1038/nmeth.2019

Singh A, Dawson B, Franich R, Cowan F, Warnes J (1999) The Relationship Between Pit Membrane Ultrastructure and Chemical Impregnability of Wood. Holzforschung 53:341–346. https://doi.org/10.1515/HF.1999.056

Sluiter A, Hames B, Ruiz R, Scarlata C, Sluiter J, Templeton D, Crocker D (2012) Determination of structural carbohydrates and lignin in biomass. National Renewable Energy Laboratory, Golden, Colorado, pp 1–15

Stone JE, Green HV (1959) Penetration and diffusion into hardwoods. Tappi 42:700–709
Stone JE, Scallan AM (1967) The Effect of Component Removal Upon the Porous Structure of the Cell Wall of Wood. II. Swelling in Water and the Fiber Saturation Point. Tappi 50:496. https://doi.org/10.32964/TJ50.10.496
Takada M, Tanaka Y, Minami E, Saka S (2016) Comparative study of the topochemistry on delignification of Japanese beech (*Fagus crenata*) in subcritical phenol and subcritical water. Holzforschung 70:1047–1053. https://doi.org/10.1515/hf-2016-0033
Takada M, Minami E, Kawamoto H (2021) Topochemistry of the delignification of Japanese beech (*Fagus crenata*) wood by supercritical methanol treatment. ACS Omega 6:20924–20930. https://doi.org/10.1021/acsomega.1c02345
Takata N, Tsuyama T, Nagano S, Baba K, Yasuda Y, Sakamoto S, Mitsuda N, Taniguchi T (2021) Prior secondary cell wall formation is required for gelatinous layer deposition and posture control in gravi-stimulated aspen. Plant J 108:725–736. https://doi.org/10.1111/tpj.15466
Viljanen M, Help H, Suhonen H, Svedström K (2023) Combined X–ray diffraction tomography imaging of tension and opposite wood tissues in young hybrid aspen saplings. Wood Sci Technol 57:797–814. https://doi.org/10.1007/s00226-023-01477-3
Wagih A, Hasani M, Hall SA, Theliander H (2021) Micro/nano-structural evolution in spruce wood during soda pulping. Holzforschung 75:754–764. https://doi.org/10.1515/hf-2020-0113
Wagih A, Hasani M, Hall SA, Novak V, Theliander H (2022) *In situ* microstructural evolution of spruce wood during soda pulping using synchrotron X-ray tomography. Holzforschung 76:611–621. https://doi.org/10.1515/hf-2021-0204
Wang J, Jiang L, Long K, Liao Z, Guo Z, Wang X (2025) In-situ characterization of the compression failure behavior of Chinese fir wood by using micro-CT and digital volume correlation analysis. Wood Sci Technol 59:85. https://doi.org/10.1007/s00226-025-01689-9
Wardrop A, Davies G (1961) Morphological factors relating to the penetration of liquids into wood. Holzforschung 15:129–141. https://doi.org/10.1515/hfsg.1961.15.5.129
Whiting P, Goring DAI (1981) The topochemistry of delignification shown by pulping middle lamella and secondary wall tissue from black spruce wood. J Wood Chem Technol 1:111–122. https://doi.org/10.1080/02773818108085108
Wojtasz-Mucha J, Hasani M, Theliander H (2017) Hydrothermal pretreatment of wood by mild steam explosion and hot water extraction. Bioresour Technol 241:120–126. https://doi.org/10.1016/j.biortech.2017.05.061
Wood JR, Ahlgren PA, Goring DAI (1972) Topochemistry in the chlorite delignification of spruce wood: the role of the hemicelluloses. Svensk Papperstidn 71:15–19
Zanuttini M, Citroni M, Marzocchi V, Inalbon C (2005) Alkali impregnation of hardwood chips. Tappi J 4:28–30
Zhang C, Fujita M, Takabe K (2004) Extracellular diffusion pathway for heartwood substances in *Albizia julibrissin* Durazz. Holzforschung 58:495–500. https://doi.org/10.1515/HF.2004.075

Authors and Affiliations

Carolina Marion de Godoy[1] · Endri Laçaj[2] · Klara Hackenstrass[3] · Luigi Galluccio[1,4] · Haiyang Yu[3] · Sara Florisson[3] · Malin Wohlert[3] · Stephen A. Hall[2] · Merima Hasani[1,4] · Hans Theliander[1,4]

✉ Merima Hasani
merima.hasani@chalmers.se

[1] Department of Chemistry and Chemical Engineering, Chalmers University of Technology, Gothenburg SE-412 96, Sweden

[2] Division of Solid Mechanics, Lund University, Lund SE-221 00, Sweden

[3] Department of Materials Science and Engineering, Uppsala University, Uppsala SE-751 03, Sweden

[4] Wallenberg Wood Science Center, Chalmers University of Technology, Gothenburg SE-412 96, Sweden